Cancer Immunology, Immunotherapy (2025) 74:132
https://doi.org/10.1007/s00262-025-03986-5

RESEARCH

NSUN2/ALYREF axis-driven m^{5}C methylation enhances PD-L1 expression and facilitates immune evasion in non-small-cell lung cancer

Yiran Yang[1] · Leiqun Cao[1] · Xin Xu[1,2] · Dan Li[1] · Yiran Deng[1] · Lan Li[1] · Bingjie Zeng[1] · Haixia Jiang[1] · Liang Shan[1] · Yiwen Huang[1] · Yunhua Xu[3] · Lifang Ma[1]

Received: 13 December 2024 / Accepted: 17 February 2025 / Published online: 3 March 2025

Abstract

Non-small-cell lung cancer (NSCLC) represents a highly prevalent form of malignancy. 5-methylcytosine (m^{5}C) methylation functions as a key post-transcriptional regulatory mechanism linked to cancer progression. The persistent expression of PD-L1 in tumor cells plays a pivotal role in facilitating immune evasion and promoting T-cell exhaustion. However, the involvement of m^{5}C in NSCLC immune evasion remains inadequately understood. This study seeks to explore the function of the m^{5}C methyltransferase NSUN2 in modulating PD-L1 expression and facilitating immune evasion in NSCLC. Our findings indicate elevated levels of NSUN2 and ALYREF in NSCLC, and both promote the growth of NSCLC cells and the progression of lung cancer. Moreover, the expression of PD-L1 in NSCLC tissues positively correlates with NSUN2 and ALYREF expression. We then discovered that PD-L1 acts as a downstream target of NSUN2-mediated m^{5}C modification in NSCLC cells. Knocking down NSUN2 significantly reduces m^{5}C modification of *PD-L1* mRNA, thereby decreasing its stability via the m^{5}C reader ALYREF-dependent manner. Furthermore, inhibiting NSUN2 enhanced CD8$^+$ T-cell activation and infiltration mediated by PD-L1, thereby boosting antitumor immunity, as confirmed in both in vitro and in vivo experiments. Collectively, these results suggested that NSUN2/ALYREF/PD-L1 axis plays a critical role in promoting NSCLC progression and tumor cell immune suppression, highlighting its potential as a novel therapeutic strategy for NSCLC immunotherapy.

Keywords m^{5}C · NSUN2 · ALYREF · PD-L1 · Immune evasion · NSCLC

Introduction

According to the Global Cancer Statistics (GLOBOCON) 2022, lung cancer stands out as the most prevalent cancer and topping the list of cancer fatalities in 2022 [1]. Non-small-cell lung cancer (NSCLC) is particularly significant among the types of lung cancer. Despite remarkable progress in surgical and locoregional therapies for NSCLC, patients diagnosed with advanced NSCLC generally face an unsatisfactory prognosis.

Recent advancements in the field of immunotherapy have shown promise in halting tumor progression and providing long-term clinical benefits for patients with malignancies [2]. Specifically, immune checkpoint inhibitors (ICBs) targeting programmed cell death protein 1 (PD-1) and its ligand PD-L1 have demonstrated broad applicability across various cancer types, leading to sustained clinical responses in cases where treatment is effective [3]. However, it is important to note that most patients with NSCLC are notal ways

Yiran Yang, Leiqun Cao and Xin Xu have contributed equally to this work.

✉ Yunhua Xu
xuyunhua1015@hotmail.com

✉ Lifang Ma
malifang0606118@126.com

[1] Department of Clinical Laboratory Medicine, Shanghai Chest Hospital, Shanghai Jiao Tong University School of Medicine, No. 241 West Huaihai Road, Shanghai 200030, China

[2] Shanghai Institute of Thoracic Oncology, Shanghai Chest Hospital, Shanghai Jiao Tong University School of Medicine, No. 241 West Huaihai Road, Shanghai 200030, China

[3] Shanghai Lung Cancer Center, Shanghai Chest Hospital, Shanghai Jiao Tong University School of Medicine, No. 241 West Huaihai Road, Shanghai 200030, China

sensitive to ICB treatments. To improve the clinical efficacy of PD-L1/PD-1 treatments in NSCLC, further exploration of the molecular mechanisms governing PD-L1 regulation is necessary.

PD-L1 is highly expressed in a variety of tumor cells. PD-L1 inhibits the functional efficacy of cytotoxic lymphocytes and their capacity to kill tumor cells, which is a key mechanism of immune evasion [4–6]. The regulation of PD-L1 involves complex and multifactorial processes, including gene transcription, transcriptional, post-transcriptional modification, and post-translational modification [7]. Among these, 5-methylcytosine (m^5C) RNA methylation, one of the post-transcriptional modifications, has been increasingly recognized for its pivotal role in controlling gene expression [8, 9]. m^5C methylation is a type of RNA modification which involves the stability and function of various RNA molecules, such as mRNA and tRNA. m^5C is regulated by m^5C methyltransferase (writers), demethylases (erasers), and m^5C-binding proteins (readers) [10]. NOP2/Sun RNA methyltransferase 2 (NSUN2), a crucial m^5C methyltransferase, exerts non-negligible roles in tumorigenesis in an m^5C-dependent manner [11–13]. Currently, it was demonstrated that NSUN2 is highly upregulated in various tumors, such as breast cancer [14], colorectal cancer [15], and gallbladder carcinoma [16], and is associated with malignant phenotypes. Additionally, NSUN2 expression has been found to be negatively associated with T-cell activation and may serve as a potential immunotherapy marker in head and neck squamous cell carcinoma (HNSC) [17]. However, the function of NSUN2 and its roles in regulating the PD-L1 expression to exert the antitumor immunity of NSCLC remain elusive.

In this study, we initially proved PD-L1 is a downstream target of NSUN2-mediated m^5C modification in NSCLC cells. We elucidated its pivotal role in facilitating immune evasion in NSCLC cells via the activation of the NSUN2/ALYREF/PD-L1 axis. Furthermore, NSUN2 regulates *PD-L1* mRNA stability in an m^5C-ALYREF-dependent manner, indicating that PD-L1 expression is modulated by m^5C modification. Our findings uncover the regulatory mechanism for PD-L1 by m^5C modification and may provide a potential therapeutic target for controlling immune escape in NSCLC.

Materials and methods

Clinical tissue samples

Clinical samples of the paired adjacent normal lung tissues and NSCLC tissues ($n = 180$) were collected from the Department of Biobank, Shanghai Chest Hospital. Tumor microarrays were constructed using tissue samples from 60 of the 180 patients. The patients' clinical characteristics information was shown in Supplementary Table 1. Written informed consents were obtained from patients. All experiments were approved by the ethics and research committees of the Shanghai Chest Hospital. The specific ethics approval number is KS23044.

Cell culture and pharmacologic drug treatment

Human NSCLC cell lines NCI-H1299, NCI-H1975, Calu-1, A549, PC9, human normal lung epithelial cells BEAS-2B, human bronchial epithelial cell line 16HBE, HEK293T, and the murine Lewis lung cancer cell (LLC) line were obtained from our previous studies [18]. All cells were maintained in DMEM (Gibco) supplemented with 10% fetal bovine serum (FBS, HyClone) and 1% penicillin/streptomycin (Invitrogen). All cells were incubated at 37 °C in a 5% CO_2 environment. All cell lines were tested negative for mycoplasma contamination. Atezolizumab (anti-PD-L1 blockade antibody; Selleck) or control IgG (Selleck) was used at 10 μg/mL for cell treatment. MY-1B (MedChemExpress) was used at a final concentration of 0–50 μM. Nivolumab (Selleck) or control IgG (Selleck) was used at 10 μg/mL for cell treatment.

Plasmids, transfection, and lentiviral transduction

Oligonucleotides encoding shRNAs that target NSUN2, including both complementary sense and antisense strands, were synthesized, annealed, and subsequently cloned into the pLKO.1 vector. The sequences of these oligonucleotides were detailed in Supplementary Table 2. Plasmids for the overexpression of ALYREF were produced by Zuorun Biotech. Transfection of the plasmids was performed utilizing Lipofectamine 2000 (Thermo Fisher Scientific). For the generation of lentiviral particles, HEK293T cells were co-transfected with the lentiviral vectors, packaging plasmid psPAX2, and envelope plasmid pMD2.G. After 48 h of transfection, the infectious lentiviral particles were collected, filtered through 0.45 μm PVDF filters, and employed to transduce and infect targeted NSCLC cells.

RNA m^5C dot blot assay

Total RNA was extracted using RNA-easy Isolation reagent (Vazyme). The mRNA was denatured by heating at 100 °C for 10 min, then immediately cooled on ice. It was subsequently transferred to Biodyne Nylon Transfer Membranes (Beyotime) and cross-linked with 365 nm UV light for 10 min. Following a 1 h block with 5% nonfat milk in PBST at room temperature, the membrane was incubated overnight at 4 °C with an anti-m^5C primary antibody (Proteintech). Afterward, it was treated with an HRP-conjugated secondary antibody for 1 h and visualized via chemiluminescence.

Methylene blue (Beyotime) served as a reference control for the RNA samples.

RNA extraction and RT-qPCR

RNA was extracted utilizing the RNA-easy Isolation reagent (Vazyme), followed by reverse transcription using HiScript III RT SuperMix (Vazyme). To measure the expression levels of the target RNAs, quantitative reverse transcription polymerase chain reaction (RT-qPCR) was conducted with the HiScript II One Step qRT-PCR SYBR Green Kit (Vazyme). The results were adjusted relative to GAPDH levels, and the mRNA quantities were determined employing the $2^{-\Delta\Delta Ct}$ method. The detailed primers are listed in Supplementary Table 2.

RNA immunoprecipitation (RIP) assay

The BeyoRIP™ RIP Assay Kit (Beyotime) was utilized following the manufacturer's protocol. First, anti-ALYREF antibody, anti-m^5C primary antibody, or control IgG was incubated with protein A/G magnetic beads for 30 min at room temperature. Then, the cell lysate supernatants were combined with the antibody-coated magnetic beads and incubated at 4 °C overnight. The next day, the complexes of cell lysate, antibody, and magnetic beads were incubated at 55 °C for 30 min. Finally, RNA was extracted using the RNA-easy Isolation reagent (Vazyme) and quantified by RT-qPCR. The primer sequences used for RIP are detailed in Supplementary Table 2.

RNA pull-down assay

Partial *PD-L1* mRNA probes, either with or without m^5C modification, were synthesized by Generay (Shanghai, China). These probes were incubated with A549 cell lysates or purified ALYREF (BIOVISION-TECH, Shanghai, China) overnight at 4 °C. The following day, streptavidin-conjugated magnetic beads (MedChemExpress) were added to the complex and incubated at room temperature for 3 h. After washing, the magnetic beads were heated, and the target protein was detected via WB.

Luciferase reporter assay

Luciferase reporter assays were performed by inserting partial *PD-L1* 3′-UTR sequences, either wild-type (WT) or with mutated (Mut) m^5C sites, into the pmir-GLO luciferase reporter plasmid (Zuorun Biotech). Luciferase activity was assessed by the Dual-Luciferase Reporter Assay Kit (Promega, Madison, WI, USA). The relative firefly luciferase activity was normalized to the Renilla luciferase activity.

mRNA stability detection

Cells were treated with Actinomycin D (ActD, 5 μg/mL, MedChemExpress) at time points of 0, 3, and 6 h before trypsinization and collection. Total RNA extraction was carried out employing the RNA-easy Isolation reagent. To evaluate the relative amounts of *PD-L1* mRNA, RT-qPCR was conducted.

Production of cytokine or protein analysis

Tissues obtained from clinical samples were homogenized in phosphate-buffered saline (PBS) with a 1 × protease inhibitor and 1% Triton X-100. The prepared homogenates were subsequently employed to assess the levels of NSUN2 or ALYREF by ELISA assay (Shanghai Enzyme-linked Biotechnology). Furthermore, the amounts of tumor necrosis factor-α (TNF-α) and interferon-γ (IFN-γ) in the supernatants of the cell cultures were determined using commercial ELISA kits (JONLNBIO).

Animal models

Athymic nude male mice (aged 4–6 weeks) and C57BL/6 male mice (aged 4–6 weeks) were sourced from Jiesijie (Shanghai, China) Biotechnology Co., Ltd. and were housed in a specific pathogen-free (SPF) animal facility located at the Shanghai Chest Hospital. All animal experiments were approved by the institutional ethics committee of Shanghai Chest Hospital. For the tumorigenesis assay, cells were injected into athymic nude mice to obtain cell line-derived xenograft (CDX) models ($n = 5$/group). Tumor growth was assessed at 10-day intervals for CDX^{A549} and at 5-day intervals for CDX^{H1975} with a digital caliper, and volume was calculated as follows: $1/2 \times L \times W^2$ (L indicates length, and W indicates width). After 4 weeks for CDX^{A549} and 2 weeks for CDX^{H1975}, the mice were euthanized, and the xenografts were subsequently weighted.

To create the Lewis lung cancer model, a total of 1×10^6 LLC cells transfected with the following constructs were injected subcutaneously into the right dorsal flank of C57BL/6 mice ($n = 5$/group). Both shNSUN2 LLC cells and control cells, with or without overexpression of ALYREF, were employed to explore the role of the NSUN2/ALYREF axis in immune evasion. Mice were inoculated with either shNSUN2 LLC cells or control cells that had received treatment with PD-L1 mAb treatment (Bio X Cell, Beijing, China) or control IgG isotype (ISO mAb, Bio X Cell) administration to evaluate the immunosuppressive impact of NSUN2 and to ascertain if this impact was reliant on PD-L1. Once the tumors became palpable, the mice were pooled and randomized. PD-L1 mAb or isotype was administered intraperitoneally every 3 days at a concentration of 100 μg

per mouse. Tumor volume was assessed every three days using calipers. Fifteen days after grouping, the mice were sacrificed, and tumor samples were collected and prepared for further analysis.

Flow cytometry

The discrimination between live and dead cells was carried out using Fixable Viability Dye (BioLegend). To block nonspecific binding of Fc receptors, single-cell suspensions were incubated with CD16/CD32 (eBioscience), and subsequently, staining was performed using antibodies in accordance with established protocols. The analysis of samples was performed using anti-human-specific antibodies sourced from BioLegend, including anti-CD45 (HI30), anti-CD8 (SK1), anti-CD3 (SK3), and anti-PD-L1 (MIH1).

Western blot (WB) analysis

For the WB analysis, proteins were extracted with a lysis buffer, then separated using 8–15% SDS-PAGE gel, and subsequently transferred to PVDF membranes. Following this, the membranes were blocked using 5% nonfat milk in PBS/Tween 20 and then incubated with the designated primary and secondary antibodies. The antibodies employed included: anti-NSUN2 (dilution of 1:1000; Immunoway), anti-ALYREF (dilution of 1:1000; Santa Cruz Biotechnology), GAPDH (dilution of 1:2000, Cell Signaling Technology), and anti-PD-L1 (dilution of 1:1000; Santa Cruz Biotechnology).

Immunohistochemistry (IHC) analysis

For IHC, slides underwent deparaffinization, rehydration, and antigen retrieval, followed by blocking of endogenous peroxidase activity. They were incubated overnight at 4 °C with antibodies against NSUN2 (1:200, Proteintech), ALYREF (1:200, Santa Cruz Biotechnology), CD8 (1:200, Santa Cruz Biotechnology), and CD4 (1:200, Santa Cruz Biotechnology). A horseradish peroxidase-conjugated secondary antibody and DAB were applied, and slides were counterstained with hematoxylin. IHC scores were calculated by multiplying staining intensity (0–3) by the positive rate (0–4), corresponding to positive area percentages.

Cell proliferation, migration, and 3D spheroid formation assays

For the cell proliferation assay, the cells were trypsinized and placed into 96-well plates at a density of 5000 cells per well. Cell proliferation was assessed every 24 h from day 1 through day 6 utilizing CCK-8 (MedChemExpress) reagent following the manufacturer's instructions. In the cell migration assay, cells were plated in 6-well plates at a concentration of 2×10^5 cells/mL. After 24 h of incubation, a sterile 1 mL pipette tip was used to create scratches in the center of the confluent monolayer, and the cells were maintained in DMEM without serum. The migration of cells into the wound area was observed using a microscope at 0 h and 24 h post-injury. For the 3D spheroid formation assay, 50 μL of Basement Membrane Extract (BME, Trevigen) was pipetted into each well of a 96-well plate and allowed to solidify at 37 °C. Following this, treated cells were placed on top of the BME-based culture system at a density of 5000 cells in 200 μL per well. The culture medium was refreshed every 3 days. After 7 days of culture, the number and size of spheroids were quantified.

PBMCs isolation and T-cell killing assay in vitro

To isolate the PBMCs, Lymphoprep (STEMCELL) was utilized according to the manufacturer's instructions. In brief, the diluted blood was meticulously layered over Lymphoprep, allowing for the retrieval of the mononuclear cell fraction from the plasma post-centrifugation. The interface from Lymphoprep was carefully collected and subsequently washed with Hanks' Balanced Salt Solution. A total of 1×10^6 PBMCs were cultured in 1 mL of RPMI supplemented with 10 ng/mL of IL-2 (R&D). A549 shCtrl and shNSUN2 cells were placed in a 96-well plate and co-cultured for 3 days with PBMCs that had previously been activated with 100 ng/mL of anti-CD3 antibody, 100 ng/mL of anti-CD28 antibody, and 10 ng/mL of IL-2. The PBMCs to A549 cell ratio during co-culture were kept at 4:1. Afterward, cell death was measured by staining with SYTOX Green followed by flow cytometry.

Statistics

GraphPad Prism was used to evaluate the data and create the corresponding graphs. For comparing two groups, the Student's unpaired *t*-test was applied. One-way or two-way analysis of variance (ANOVA) was performed to evaluate the statistical significance of differences among two groups. Correlations were analyzed using the Pearson correlation test and Spearman rank-correlation analysis. Survival curves were obtained by using the Kaplan–Meier method, and comparisons were made by using a log-rank test. The data are consistently presented as the mean ± SD. A significance level of $p < 0.05$ was established for all tests.

Results

NSUN2 and ALYREF were significantly upregulated in NSCLC patients and NSCLC cell lines

To investigate the potential role of m^5C modification in the progression of NSCLC, we performed a preliminary analysis of the m^5C regulatory genes expression using data from The Cancer Genome Atlas (TCGA). Our analysis revealed obvious differences in the expression of m^5C methyltransferase NSUN2 and m^5C-binding proteins ALYREF between the NSCLC tumor tissues and adjacent normal tissues (ANTs) (Fig. 1A, B). In addition, both NSUN2 and ALYREF were notably upregulated in pan-cancer analyses compared to ANTs, with particularly pronounced variability in lung squamous cell carcinoma (LUSC) and lung adenocarcinoma (LUAD) (Supplementary Fig. 1A). These results were corroborated across various NSCLC datasets including GSCA and UALCAN database (Fig. 1C D, Supplementary Fig. 1B). To further validate these observations, we analyzed the expression of NSUN2 and ALYREF in the normal bronchial epithelial cell lines 16HBE and BEAS-2B, as well as in multiple NSCLC cell lines. As shown in Fig. 1E, NSUN2 and ALYREF were significantly upregulated in NSCLC cells compared to 16HBE and BEAS-2B. Additionally, we assessed the protein levels of NSUN2 and ALYREF in NSCLC samples and found that their expression was significantly higher in NSCLC tumors than ANTs, as demonstrated by immunohistochemical staining (IHC) (Fig. 1F, G) and Western blot (WB) (Fig. 1H). Furthermore, dot blot analyses revealed that m^5C levels in NSCLC tumor tissues were significantly elevated relative to ANTs, correlating with the expression levels of NSUN2 and ALYREF (Fig. 1H). Collectively, these findings suggest that NSUN2 and ALYREF expression are upregulated and positively correlated with m^5C levels in NSCLC tissues.

NSUN2 promotes the proliferation of NSCLC both in vitro and in vivo

To further demonstrate the influence of NSUN2 in NSCLC progression, we selected H1299 and A549 cell lines which exhibit higher expressed NSUN2 to perform NSUN2 knockdown. Subsequently, the efficiency of NSUN2 knockdown was confirmed through WB and RT-qPCR analysis (Fig. 2A and Supplementary Fig. 2A). Following NSUN2 knockdown, we assessed the growth rate, three-dimensional (3D) spheroid formation, and colony-forming capacity of H1299 and A549 cell lines. Notably, the CCK-8 assay demonstrated that reduced NSUN2 expression significantly slowed cell proliferation in both H1299 and A549 cell lines (Fig. 2B). Furthermore, the 3D spheroid assay revealed fewer and smaller spheroids upon NSUN2 downregulation (Fig. 2C, D). Colony formation experiments, conducted to examine the extended effects of NSUN2 on cell proliferation, indicated a reduction in colony numbers in the knockdown group (Fig. 2E, F). Additionally, scratch and transwell assays showed that NSUN2 suppression impaired the migration and invasion abilities of H1299 and A549 cells (Supplementary Fig. 2B–D). Collectively, these results underscore the role of NSUN2 in enhancing NSCLC cell proliferation, migration, and invasion in vitro.

For in vivo analysis, NSUN2 knockdown and control cells were subcutaneously injected into nude mice to evaluate its effect on xenograft tumor development. Compared to the control group, NSUN2 knockdown tumors exhibited significantly reduced size and weight after 30 days post-transplantation (Fig. 2G–I). In summary, our data suggest that NSUN2 may function as an oncogenic driver, promoting the growth and metastatic potential of NSCLC.

ALYREF expression is positively correlated with NSUN2 expression, and both serve as poor prognostic indicators for NSCLC patients

Given the concurrent elevation of NSUN2 and ALYREF in NSCLC, we further investigated the relationship between these two genes. First, we analyzed protein expression levels of NSUN2 and ALYREF in 180 paired NSCLC and ANTs using enzyme-linked immunosorbent assay (ELISA). The ELISA results indicated that NSUN2 and ALYREF protein levels were significantly higher in NSCLC samples compared to ANTs (Fig. 3A, B). Furthermore, we detected a positive correlation between NSUN2 and ALYREF within the NSCLC tumor tissues (Fig. 3C). This association was validated by analyses from TCGA and TIMER datasets for NSCLC, LUAD, and LUSC (Fig. 3D–H). NSUN2 expression displayed no significant association with clinical stage, while ALYREF expression showed a clear correlation (Supplementary Fig. 3A and B). We also investigated the impact of NSUN2 and ALYREF expression levels on NSCLC patient prognosis. Kaplan–Meier analysis indicated that patients with elevated NSUN2 or ALYREF expression had poorer overall survival (OS), faster progression (FP), and shorter post-progression survival (PPS) (Fig. 3I, J, Supplementary Fig. 3C–F). To further validate the association between NSUN2 and ALYREF expression and patient prognosis, we utilized the GSE31210 dataset from the GEO database, which includes gene expression data from 226 primary lung adenocarcinoma samples. The results of this external validation showed that elevated expression of

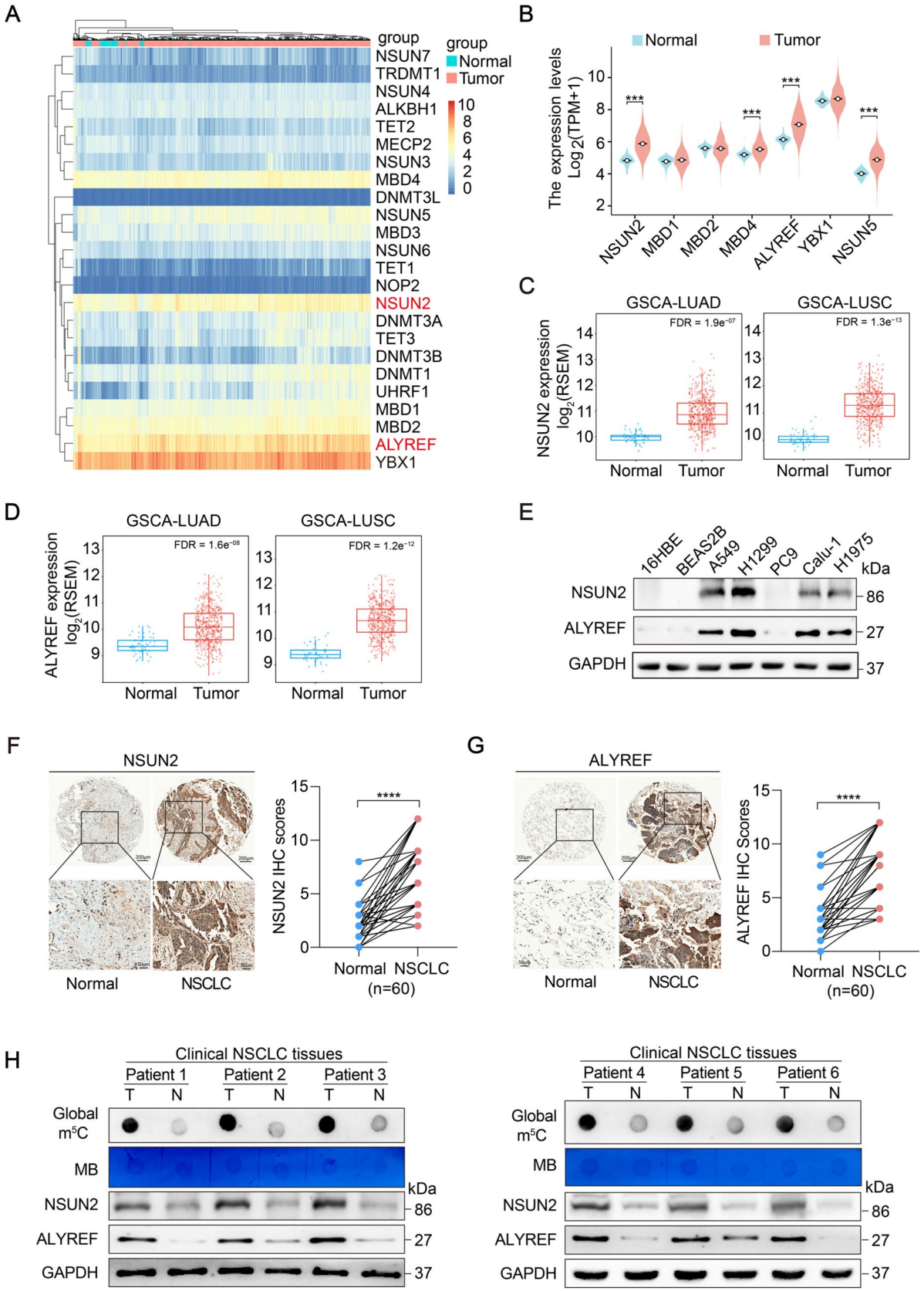
A
group
Normal
Tumor
NSUN7
TRDMT1
NSUN4
ALKBH1
TET2
MECP2
NSUN3
MBD4
DNMT3L
NSUN5
MBD3
NSUN6
TET1
NOP2
NSUN2
DNMT3A
TET3
DNMT3B
DNMT1
UHRF1
MBD1
MBD2
ALYREF
YBX1
B
Normal
Tumor
The expression levels Log2(TPM+1)
NSUN2
MBD1
MBD2
MBD4
ALYREF
YBX1
NSUN5
C
GSCA-LUAD
GSCA-LUSC
FDR = 1.9e−07
FDR = 1.3e−13
NSUN2 expression log2(RSEM)
Normal
Tumor
D
GSCA-LUAD
GSCA-LUSC
FDR = 1.6e−08
FDR = 1.2e−12
ALYREF expression log2(RSEM)
Normal
Tumor
E
16HBE
BEAS2B
A549
H1299
PC9
Calu-1
H1975
kDa
NSUN2
ALYREF
GAPDH
86
27
37
F
NSUN2
NSUN2 IHC scores
Normal
NSCLC
Normal NSCLC (n=60)
G
ALYREF
ALYREF IHC Scores
Normal
NSCLC
Normal NSCLC (n=60)
H
Clinical NSCLC tissues
Patient 1
Patient 2
Patient 3
Patient 4
Patient 5
Patient 6
T
N
Global m5C
MB
NSUN2
ALYREF
GAPDH
kDa
86
27
37

◂**Fig. 1** m^5C regulator NSUN2 and ALYREF were upregulated in NSCLC. **A**, **B** Heatmap (**A**) and Violin plot (**B**) showed the expression levels of several m^5C regulated genes in NSCLC and normal lung tissues from the TCGA. **C**, **D** The mRNA expression levels of *NSUN2* and *ALYREF* in normal lung tissues, LUAD and LUSC tissues from GSCA database. **E** The protein levels of NSUN2 and ALYREF were analyzed in human bronchial epithelial cell line 16HBE, human lung epithelial cell line BEAS-2B, human NSCLC cell lines A549, H1299, PC9, Calu1, and H1975 by WB assay. **F**, **G** The representative TMA-IHC staining images and analysis the IHC score of NSUN2 and ALYREF in paired NSCLC and ANTs ($n=60$. Scale bars: 200 μm and 50 μm). **H** The global m^5C levels, NSUN2 and ALYREF protein levels were measured by dot blot and WB assay in paired NSCLC samples and ANTs. Methylene blue staining served as the internal control. $^{***}p<0.001$ and $^{****}p<0.0001$

NSUN2 and ALYREF is significantly associated with poor patient prognosis (Supplementary Fig. 3G and H). These findings suggest that elevated NSUN2 expression may serve as an independent prognostic marker for NSCLC, and a positive correlation identified between NSUN2 and ALYREF expression.

NSUN2 and ALYREF were closely associated with the immune cell infiltration and PD-L1 expression in NSCLC

In order to further study the correlation between NSUN2 or ALYREF and tumor microenvironment immune cell infiltration, we first calculated the score of 24 immune cells' infiltration using LUSC and LUAD TCGA database. Findings indicated associations between NSUN2 or ALYREF and some tumor-infiltrating lymphocytes (TILs) in LUAD and LUSC, including Th17 cells, Th1 cells, $CD8^+$ T cells, mast cells, and macrophages (Fig. 4A, B, Supplementary Fig. 4A and B). Notably, a significant inverse correlation was observed between the expression of NSUN2 or ALYREF and $CD8^+$ T-cell infiltration, while no significant correlation was identified with $CD4^+$ T-cell infiltration (Fig. 4C, D, Supplementary Fig. 4C–H).

We then used Gendoma to explore potential interactions between NSUN2 or ALYREF and the immunosuppressive checkpoint PD-L1. Results indicated that the NSUN2 gene does not directly interact with PD-L1, while ALYREF does (Fig. 4E, F). Analysis with TIMER further revealed a negative correlation between NSUN2 or ALYREF expression and PD-L1 levels in LUAD and LUSC tumor tissues (Fig. 4G–H). Subsequently, *PD-L1* mRNA expression levels were classified and analyzed based on varying levels of NSUN2 and ALYREF within the LUAD and LUSC TCGA datasets. The results showed that NSCLC tumor tissues with higher expression of NSUN2 or ALYREF exhibited elevated PD-L1 levels, while tissues with lower NSUN2 or ALYREF expression showed reduced PD-L1 expression (Fig. 4I–L). Collectively, these findings suggest that NSUN2 and ALYREF may play a role in modulating the immune response through the regulation of PD-L1 expression.

Elevated ALYREF expression enhances the proliferation of NSCLC cells

With the observed upregulation of ALYREF in NSCLC tissues, we investigated its potential role in promoting NSCLC cell proliferation, both in vitro and in vivo. We overexpressed the wild-type ALYREF (ALYREF-WT) and a catalytically inactive mutant (ALYREF-Mut) in H1975 and Calu1 cell lines. Successful overexpression of ALYREF and its mutant variants were confirmed through WB and RT-qPCR analyses (Fig. 5A, Supplementary Fig. 5A). Growth curves generated from CCK-8 and cell counting assays demonstrated that ALYREF-WT, but not ALYREF-Mut, significantly enhanced the proliferation of H1975 and Calu1 cells compared to control cells (Empty) (Fig. 5B, C, Supplementary Fig. 5B and C). These results were further supported by findings from 3D spheroid formation and clonogenic assays, which showed similar trends in cell proliferation consistent with those observed in the CCK-8 assay (Fig. 5D–G).

Given these in vitro observations, we expanded our investigation to assess the role of ALYREF in vivo. Using a xenograft model, we found that ALYREF-WT markedly increased lung tumor growth, as reflected by tumor size and weight; however, ALYREF-Mut did not produce comparable effects (Fig. 5H–J). Thus, these findings suggest that ALYREF overexpression promotes NSCLC progression in vitro and in vivo.

NSUN2 and ALYREF mediates PD-L1 expression by regulating *PD-L1* mRNA stability in an m^5C-dependent manner

Our previous study demonstrated a positive correlation between PD-L1 expression and the levels of NSUN2 and ALYREF. NSUN2 acts as m^5C methyltransferase (writer) [19], while ALYREF functions as an m^5C binding protein (reader) [11], both recently confirmed to regulate m^5C-modified transcripts [11, 19]. Thus, we further tested whether NSUN2 and ALYREF exerted regulatory effects on PD-L1 expression in an m^5C-dependent manner. To test this hypothesis, we used NSCLC cells with NSUN2 knockdown (H1299 and A549) and cells overexpressing ALYREF (H1975 and Calu1) to measure PD-L1 expression. Knockdown of NSUN2 in H1299 and A549 cells led to reduced *PD-L1* protein and mRNA levels (Fig. 6A, B, Supplementary Fig. 6A and B). Additionally, flow cytometry (FCM) confirmed decreased PD-L1 expression on the cell surface (Fig. 6C, Supplementary Fig. 6C). In contrast, overexpression of ALYREF, but not its mutant form, significantly

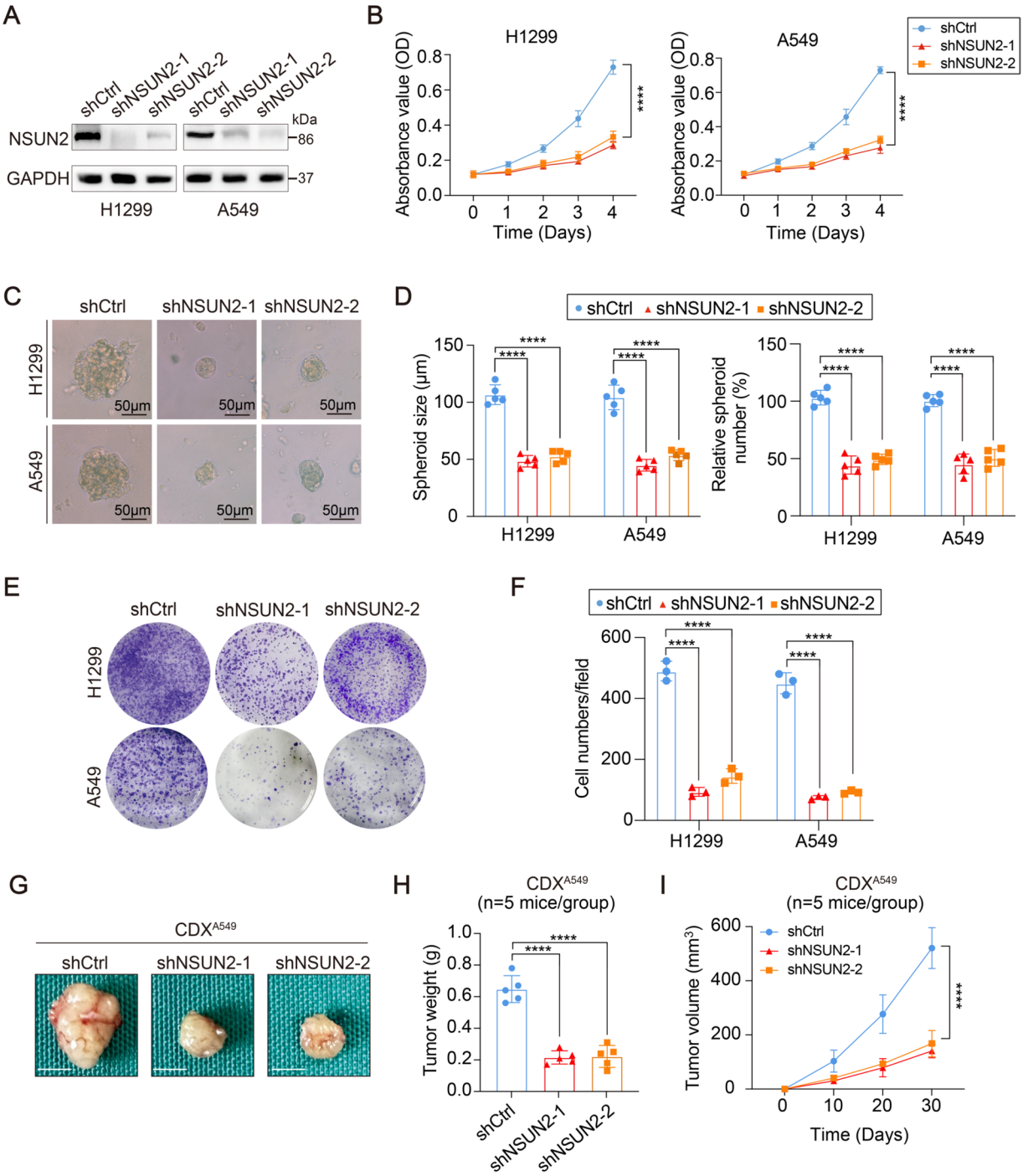

Fig. 2 Knockdown NSUN2 can restrain NSCLC tumorigenesis in vitro and in vivo. **A** NSUN2 protein expression in H1299 and A549 cell lines after NSUN2 knockdown was measured by WB assay. **B** CCK-8 assay was used to evaluate the growth ability of H1299 and A549 cells with or without NSUN2 knockdown. **C**, **D** Representative bright-field images, sizes, and relative numbers of three-dimensional (3D) spheroids generation assays which showing the effect of NSUN2 knockdown on H1299 and A549 cells growth. Scale bar, 50 μm. **E**, **F** Colony formation assays showed the effect of NSUN2 knockdown on H1299 and A549 cells growth. **G**–**I** The representative xenograft images, tumor weight, and tumor volume were analyzed in indicated groups and time points ($n = 5$/group). Scale bar, 0.5 cm. ****$p < 0.0001$

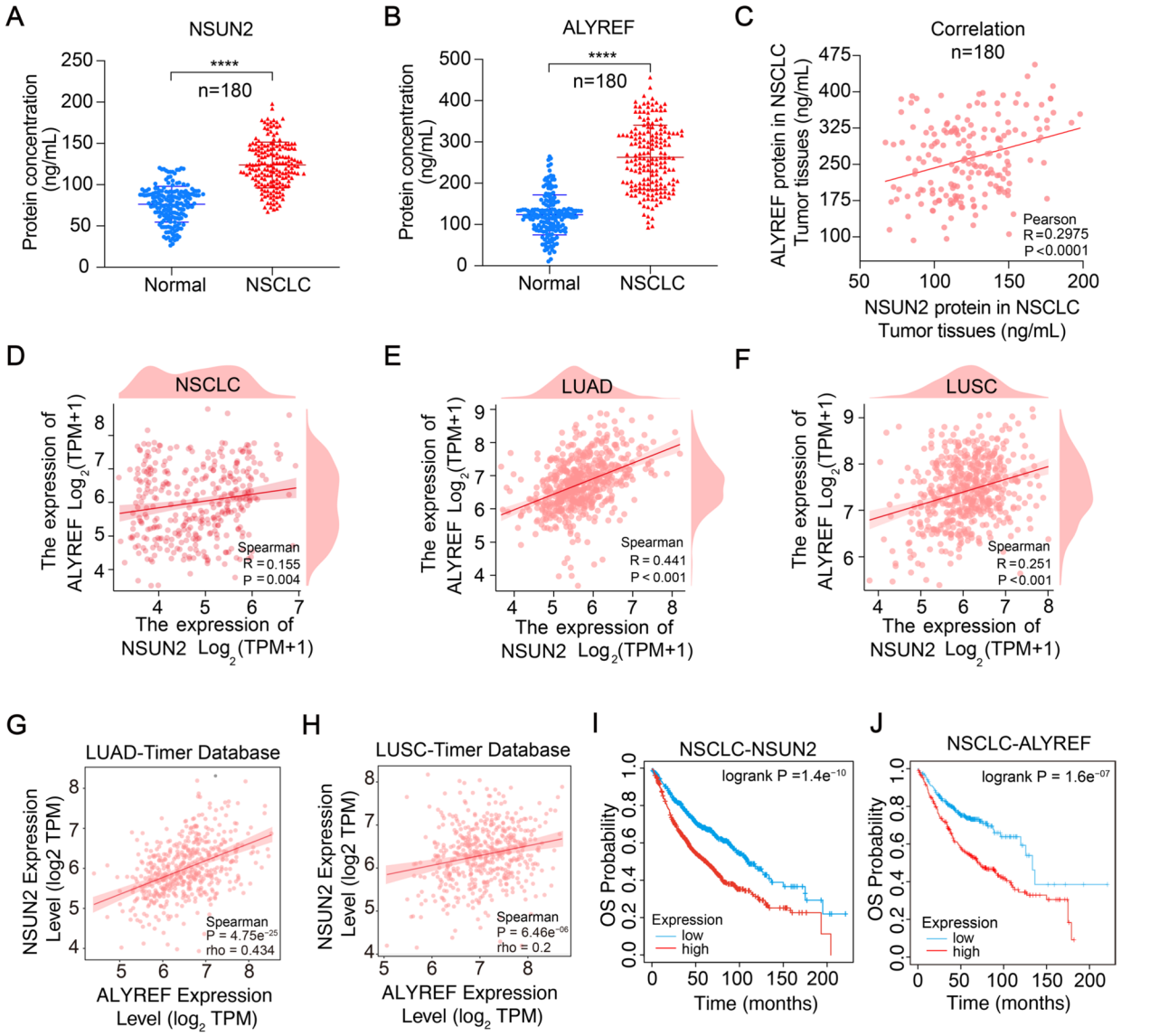

Fig. 3 NSUN2 and ALYREF are positively correlated in NSCLC. **A**, **B** NSUN2 and ALYREF protein levels were measured by ELISA assay in NSCLC and paired adjacent normal lung tissues ($n = 180$). **C** Scatter plot showing correlation between NSUN2 and ALYREF protein expression levels in tumor tissues of 180 paired NSCLC patients. $p < 0.0001$. **D**–**F** The correlation between NSUN2 and ALYREF expression in TCGA-LUAD, TCGA-LUSC, and sum of the two. $p < 0.05$. **G**, **H** The correlation between NSUN2 and ALYREF in LUAD and LUSC patients was also obtained from Timer database. **I**, **J** The overall survival (OS) based on NSUN2 and ALYREF expression in NSCLC was extracted from the Kaplan–Meier Plotter database. ****$p < 0.0001$

increased *PD-L1* protein, mRNA, and cell surface levels (Fig. 6D–F, Supplementary Fig. 6 D–F). These findings indicate that NSUN2 and ALYREF jointly regulate PD-L1 expression.

To further explore whether ALYREF interacts directly with m^{5}C-methylated *PD-L1* mRNA, we used RNA m^{5}C finder online database to identify the potential m^{5}C recognition sites on the *PD-L1* mRNA. We identified 3175C within 3′-UTR region of *PD-L1* mRNA (Fig. 6G). Based on this prediction, we performed RIP assay using anti-m^{5}C antibodies revealed that 3175C was accessible for m^{5}C modification (Fig. 6H). Specifically, we conducted pull-down assays, where we observed that the mutation of the m^{5}C modification sites significantly reduced the binding affinity between *ALYREF* and *PD-L1* mRNA (Supplementary Fig. 6G). RIP-qPCR assay showed that a decrease in m^{5}C-modified *PD-L1* mRNA following NSUN2 knockdown in H1299 and A549 cells, whereas ALYREF overexpression increased m^{5}C-modified *PD-L1* mRNA levels in H1975 and Calu1 cells (Fig. 6I, J, Supplementary Fig. 6H and I). Additionally, NSUN2 knockdown reduced ALYREF binding enrichment with *PD-L1* mRNA in A549 cells, while ALYREF

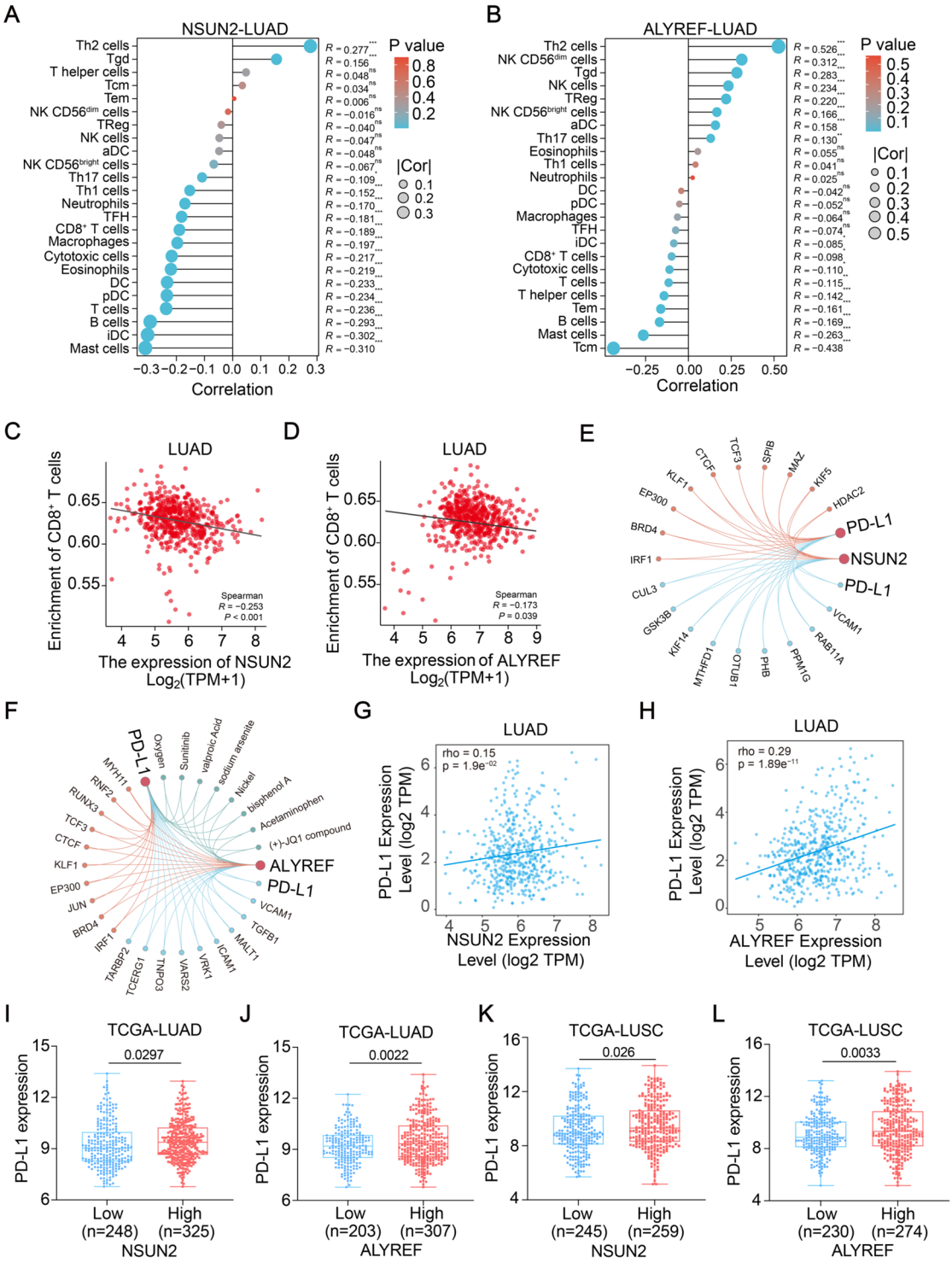

Fig. 4 NSUN2 and ALYREF expression are highly associated with immune infiltration in NSCLC. **A**, **B** Correlation between the NSUN2 or ALYREF expression level and relative abundances of 24 types of immune cells in TCGA-LUAD cohorts. The size of dots indicates the absolute value of Spearman R. **C**, **D** The correlation between NSUN2 or ALYREF expression levels and infiltration of $CD8^+$ T cells was obtained from TCGA-LUAD. **E**, **F** Correlation generegulatory network of NSUN2 or ALYREF and PD-L1 was retrieved from Gendoma web server (https://ai.citexs.com). **G**, **H** Analysis of correlations between NSUN2 or ALYREF expression and PD-L1 expression from TIMER database. **I**–**L** Correlation of NSUN2 or ALYREF and PD-L1 expression in human LUAD and LUSC tissues from TCGA dataset. $*p < 0.05$, $**p < 0.01$, and $***p < 0.001$, N.S. means no significance

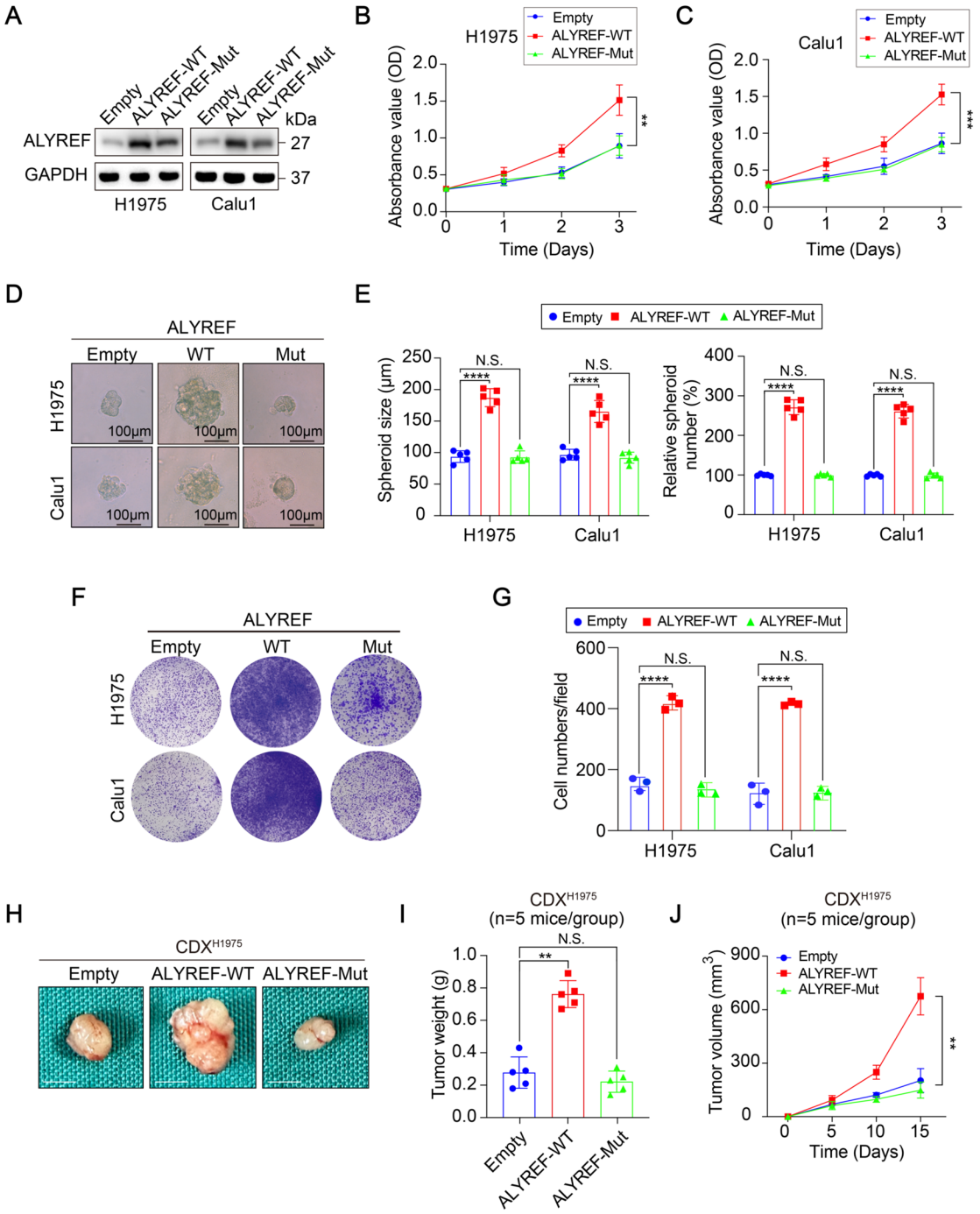

Fig. 5 Overexpression of ALYREF promotes malignant growth of NSCLC. **A** ALYREF overexpression efficiency was validated in H1975 and Calu1 cells by WB assay. **B**, **C** CCK-8 assays were used to evaluate the growth of H1975 and Calu1 cells with or without ALYREF overexpression. **D**, **E** Representative spheroid images (**D**), spheroid sizes (**E**, left panel), and spheroid numbers (**E**, right panel) of 3D spheroids generated by empty, ALYREF-WT or ALYREF-Mut H1975, and Calu1 cells. Scale bar: 100 μm. **F**, **G** Colony formation assays showing the effect of ALYREF-WT or ALYREF-Mut on H1975 and Calu1 cells growth. **H–J** The representative xenograft images, tumor weight, and tumor volume were analyzed in indicated groups and time points ($n=5$/group). Scale bar, 0.5 cm. $^{**}p<0.01$, $^{***}p<0.001$, and $^{****}p<0.0001$, N.S. means no significance

overexpression enhanced this interaction in H1975 cells (Fig. 6K, L). These findings suggest that NSUN2, through ALYREF, regulates the m^{5}C modification of *PD-L1* mRNA.

Since ALYREF is known to affect RNA stability [20], we investigated whether m^{5}C modification mediated by ALYREF influences *PD-L1* mRNA stability. By inhibiting

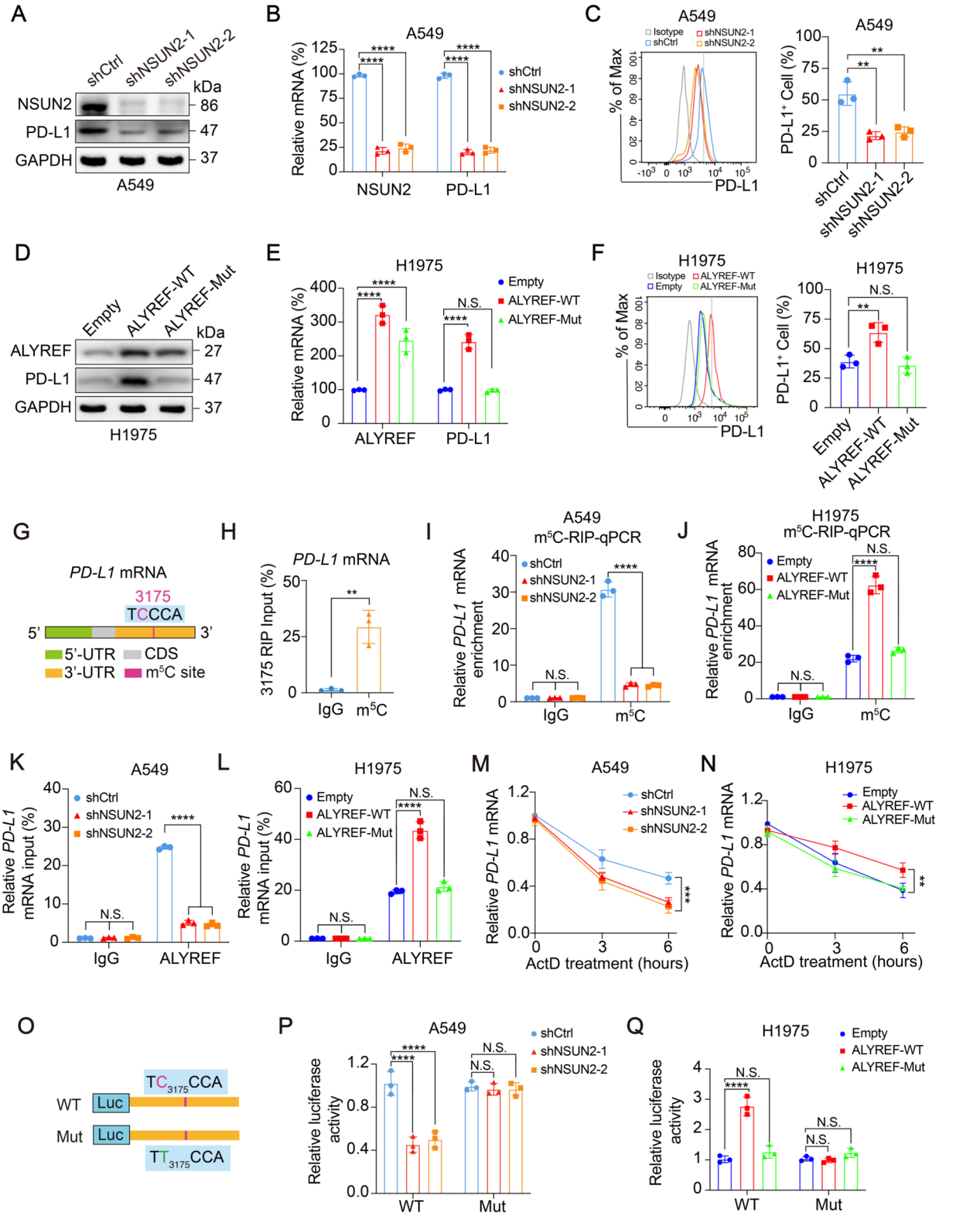

new RNA synthesis using actinomycin D, we observed that NSUN2 knockdown accelerated *PD-L1* mRNA degradation, while stable overexpression of ALYREF significantly enhanced its stability (Fig. 6M, N, Supplementary Fig. 6J and K). Additionally, we performed a luciferase reporter assay using the wild-type (WT) and mutant *PD-L1* mRNA 3′-UTR sequences, which demonstrated that the putative m^5C sites positively affected the mRNA stability of

◂**Fig. 6** NSUN2 and ALYREF positively regulate PD-L1 expression in human NSCLC cell lines. **A**, **B** The mRNA and protein expression of *PD-L1* was detected in A549 cell lines after NSUN2 knockdown by WB and RT-qPCR assay. **C** The cell membranous PD-L1 levels were measured using flow cytometry (FCM) assay. **D**, **E** The mRNA and protein expression of *PD-L1* was detected in H1975 cell lines after ALYREF-WT or ALYREF-Mut using WB and RT-qPCR assay. **F** H1975 membranous PD-L1 levels were detected by FCM assay. **G** Prediction of potential m^5C site in *PD-L1* mRNA with the RNA m^5C finder online database. **H** Candidate sites were verified with m^5C-RIP experiments. **I**, **J** m^5C modification levels of *PD-L1* mRNA were assessed by RIP assays in A549 cells with or without NSUN2 knockdown and H1975 with or without ALYREF overexpression. IgG antibodies were used as negative controls. **K**, **L** The interaction between *ALYREF* and *PD-L1* mRNA in A549 cells with or without NSUN2 knockdown and H1975 with or without ALYREF overexpression was detected by RIP assays. The enrichment of *PD-L1* was tested by RT-qPCR. **M**, **N** RT-qPCR assay was used to analyze *PD-L1* mRNA levels in A549 and H1975 cells after actinomycin D (ActD) treatment. **O** Schematic illustration of the putative m^5C sites and their mutants (Mut) in the 3′-UTR sequence of *PD-L1* mRNA. **P**, **Q** Relative luciferase activity in control, NSUN2 knockdown A549 and ALYREF-WT, ALYREF-Mut H1975 cells co-transfected with WT or mut PD-L1 (C mut to T). $^{**}p<0.01$, $^{***}p<0.001$, and $^{****}p<0.0001$, N.S. means no significance

PD-L1 via NSUN2 and ALYREF in A549 and H1975 cells (Fig. 6O–Q). Together, these results suggest that NSUN2/ALYREF maintained the stability of *PD-L1* mRNA via an m^5C-dependent mechanism.

NSUN2/ALYREF axis downregulates antitumor immunity in NSCLC

Tumor-derived PD-L1 plays a critical role in inhibiting antitumor T-cell activation. To elucidate the contributions of NSUN2 and ALYREF in PD-L1-mediated tumor immune evasion, we co-cultured $CD8^+$ T cells with NSCLC cell lines. The results indicated that knocking down NSUN2 or administering the PD-L1 inhibitor atezolizumab significantly enhanced the sensitivity of NSCLC cells to T-cell-mediated cytotoxicity compared to control groups (Fig. 7A). Furthermore, T-cell activation was evidenced by increased secretion of IFN-γ and TNF-α resulting from NSUN2 knockdown or adding atezolizumab treatment (Fig. 7B, C). In contrast, overexpression of ALYREF diminished the sensitivity of NSCLC cells to T-cell killing and led to decreased levels of IFN-γ and TNF-α; however, treatment with atezolizumab treatment could reverse these effects (Fig. 7D–F). These findings indicate that PD-L1 may serve as a pivotal mediator of the tumor immune escape mechanisms induced by NSUN2 and ALYREF in NSCLC cells.

To assess whether the immunosuppressive roles of NSUN2 and ALYREF were mediated by PD-L1 in vivo, we utilized Lewis lung carcinoma (LLC) cells exhibiting stable NSUN2 knockdown, ALYREF overexpression, or both. These modified cells were subcutaneously implanted into immunocompetent C57BL/6 mice, either with or without PD-L1 mAb treatment as illustrated in Fig. 7G. The knockdown of NSUN2 effectively inhibited tumor growth (weight and volume), mirroring the effects seen with PD-L1 blockade. Importantly, overexpression of ALYREF did not rescue tumor growth (Fig. 7H, Supplementary Fig. 7A). In contrast, when ALYREF was overexpressed alone, tumor growth increased, but this effect was reversible with PD-L1 mAb treatment (Fig. 7H, Supplementary Fig. 7A).

Next, we assessed $CD8^+$ T-cell infiltration in Lewis lung carcinoma by FCM. Both NSUN2 knockdown and anti-PD-L1 therapy significantly reduced $CD8^+$ T-cell infiltration proportion in tumors compared to control groups, while overexpression of ALYREF did not ameliorate this effect (Fig. 7I). Furthermore, ALYREF overexpression alone was associated with decreased $CD8^+$ T-cell infiltration, but anti-PD-L1 treatment restored this infiltration. These results were corroborated by IHC staining, although no significant differences were observed in $CD4^+$ T-cell infiltration (Fig. 7J, Supplementary Fig. 7B–D).

To further investigate the potential of NSUN2 as a therapeutic target, we first assessed the specificity and toxicity of the NSUN2 inhibitor MY-1B. H1299 and A549 cells were treated with MY-1B, and the resulting changes in NSUN2 protein and RNA levels were quantified. Additionally, we evaluated the cytotoxicity of MY-1B over a range of concentrations. The results demonstrated that MY-1B treatment significantly reduced both NSUN2 protein and RNA levels in H1299 and A549 cells (Supplementary Fig. 7E and F). Moreover, MY-1B displayed dose-dependent cytotoxicity in tumor cells, while exhibiting no significant toxicity to normal lung epithelial BEAS2B cells (Supplementary Fig. 7G). These experiments highlight the targeted inhibition of NSUN2 and suggest that the NSUN2 inhibitor has a selective cytotoxic effect on NSCLC cells. Then, we treated H1299 cells with the MY-1B in combination with the PD-1 inhibitor and performed co-culture experiments with activated PBMCs. To assess the effects of the combination immunotherapy on tumor cell viability, we conducted CCK-8 assays. The results demonstrated that the combination treatment significantly reduced H1299 cell viability compared to the single-agent treatments, indicating a synergistic effect between NSUN2 inhibition and PD-1 blockade in enhancing antitumor activity (Supplementary Fig. 7H). These findings support the potential of combining NSUN2 inhibitors with PD-1 inhibitors for improving the efficacy of immune-based therapies.

In summary, these findings indicate that NSUN2 and ALYREF contribute to tumor immune escape through the upregulation of PD-L1, which inhibits $CD8^+$ T-cell infiltration within the tumor microenvironment. The effects of NSUN2 knockdown mimic those observed with PD-L1 blockade, highlighting a potential therapeutic target in

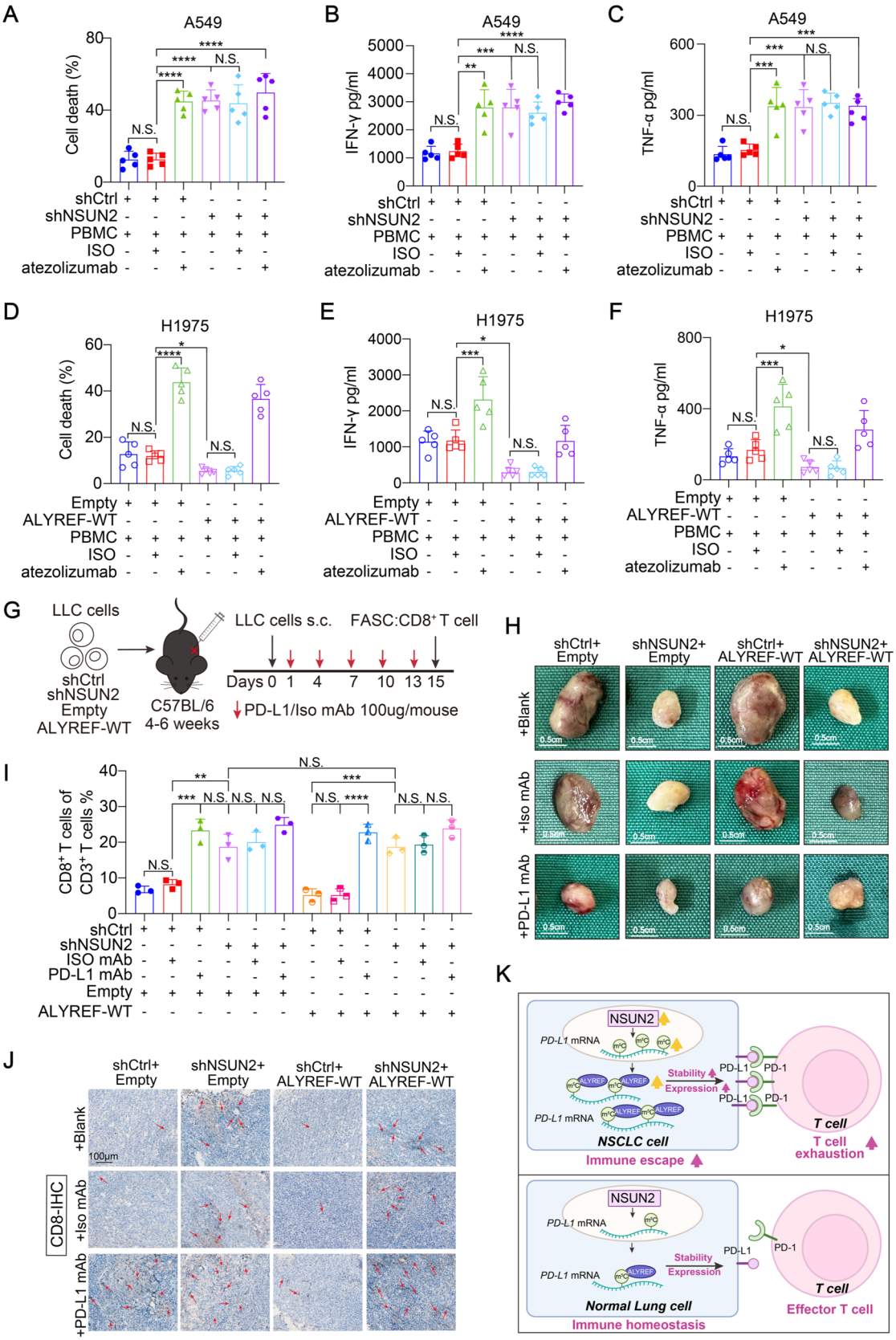
A
A549
Cell death (%)
shCtrl
shNSUN2
PBMC
ISO
atezolizumab
B
A549
IFN-γ pg/ml
C
A549
TNF-α pg/ml
D
H1975
Cell death (%)
Empty
ALYREF-WT
E
H1975
IFN-γ pg/ml
F
H1975
TNF-α pg/ml
G
LLC cells
shCtrl
shNSUN2
Empty
ALYREF-WT
C57BL/6
4-6 weeks
LLC cells s.c.
FASC:CD8⁺ T cell
Days 0 1 4 7 10 13 15
PD-L1/Iso mAb 100ug/mouse
H
shCtrl+ Empty
shNSUN2+ Empty
shCtrl+ ALYREF-WT
shNSUN2+ ALYREF-WT
+Blank
+Iso mAb
+PD-L1 mAb
I
CD8⁺ T cells of CD3⁺ T cells %
ISO mAb
PD-L1 mAb
J
CD8-IHC
100μm
K
NSUN2
PD-L1 mRNA
Stability
Expression
PD-L1
PD-1
NSCLC cell
Immune escape
T cell
T cell exhaustion
Normal Lung cell
Immune homeostasis
Effector T cell

◂**Fig. 7** NSUN2/ALYREF axis suppresses antitumor T-cell immunity by upregulating *PD-L1* mRNA. **A**, **D** Relative cell death of the indicated A549/H1975 cells after coculturing with PBMCs (PBMC:NSCLC cells = 4:1). **B**, **C**, **E**, **F** The IFN-γ and TNF-α protein levels in co-culture medium were measured by ELISA after 48 h co-incubation. **G** Schematic diagram exhibiting the groups and treatment plan of the mouse model. **H** Images at the end points of subcutaneous tumors formed by LLC cells in C57BL/6 mice (scale bar, 0.5 cm). **I** Infiltrated $CD8^+$ T cells in $CD3^+$ T cells proportion in indicated groups were measured by flow cytometry analysis. **J** $CD8^+$ T cells densities were determined by IHC analysis in Lewis lung tumors. Scale bar, 100 μm. **K** A schematic model illustrating the mechanism of NSUN2/ALYREF axis-mediated m^5C modification of *PD-L1* mRNA promotes the NSCLC immune escape. $^*p < 0.05$, $^{**}p < 0.01$, $^{***}p < 0.001$, and $^{****}p < 0.0001$, N.S. means no significance

NSCLC. These experiments underscore the selective inhibition of NSUN2 and suggest that the NSUN2 inhibitor exerts a cytotoxic effect specifically on NSCLC cells. Furthermore, they provide a deeper insight into the potential of NSUN2 inhibitors for use in combination therapies.

Discussion

The limited efficacy of anti-PD-1/PD-L1 immunotherapy in NSCLC underscores the critical need to further elucidate the molecular mechanisms regulating PD-L1 expression and immune evasion in NSCLC [21–23]. In this study, we investigated the role of the NSUN2/ALYREF axis in modulating PD-L1 expression in m^5C-dependent way and its subsequent influence on immune escape in NSCLC (Fig. 7K). To the best of our knowledge, this is the first report demonstrating that the NSUN2/ALYREF axis upregulates PD-L1 expression in NSCLC.

The m^5C methylation modification is among the most prevalent RNA modifications in eukaryotes, playing a crucial role in epigenetic gene regulation through distinct molecular pathways [24]. Emerging evidence indicates that m^5C modification is essential in both normal physiological and pathological contexts, with particular significance in cancer development and progression [25, 26]. The biological functions of m^5C methylation are mediated by methyltransferase "writers," including members of the NSUN and DNMT families, and can be dynamically modulated by "erasers" such as the TET family, along with "reader" proteins such as ALYREF and YBX1 [11, 27–29]. Accumulating evidence indicates that NSUN2, a key m^5C methylation "writer," regulates various oncogenic pathways in cancer, including those related to cell proliferation, metastasis, and drug resistance [12, 30–32]. Numerous studies have identified NSUN2 as an oncogene in multiple cancer types. However, the specific function of NSUN2-mediated m^5C modification in NSCLC remains insufficiently understood. In this study, we first examined the expression profiles of m^5C regulatory factors in NSCLC tissues. Our analyses, based on both TCGA-NSCLC data and our own NSCLC clinical cohorts, revealed significantly elevated levels of NSUN2 and ALYREF in tumor tissues compared to ANTs, consistent with prior findings in other cancer [32–34]. This upregulation was positively associated with m^5C levels and inversely correlated with overall prognosis in NSCLC patients. Additionally, both in vitro assays and murine models, reduced NSUN2 expression was found to suppress the malignant characteristics of NSCLC cells, while ALYREF overexpression promoted tumorigenic behaviors. Collectively, these results identify NSUN2 and ALYREF as oncogenic drivers in NSCLC tumorigenesis, providing novel insights into the molecular mechanisms underlying NSCLC progression.

The critical role of tumor immunity in cancer progression is well established [35, 36], and m^5C modification has been implicated in regulating immune responses within tumors. Recent studies have demonstrated that NSUN2 negatively influences immune cell infiltration within the tumor microenvironment (TME) of prostate cancer [37]. NSUN2 also had been verified as a glucose sensor, and its activation by glucose promotes tumorigenesis and resistance to immunotherapy by sustaining TREX2 expression, thereby inhibiting the cGAS/STING pathway [34]. Numerous studies have demonstrated that patients exhibiting high PD-L1 expression on tumor cells tend to benefit from PD-1/PD-L1 antibody therapy [23, 38, 39]. Therefore, identifying strategies to modulate PD-L1 expression is of paramount importance. Leveraging RNA-seq data from the TCGA-LUAD and TCGA-LUSC databases, we identified a negative correlation between NSUN2 or ALYREF expression and both $CD8^+$ T-cell infiltration and PD-L1 expression, suggesting a potential role in modulating antitumor immunity and immune cell infiltration. NSUN2 and ALYREF have been recently validated as regulators of m^5C-modified transcripts [11, 19]. Based on our findings, we propose PD-L1 as a downstream target of m^5C modification mediated by NSUN2 and ALYREF in NSCLC cells. Indeed, NSUN2 inhibition resulted in PD-L1 downregulation and reduced m^5C binding to *PD-L1* mRNA, as confirmed through WB, RT-qPCR, flow cytometry, and m^5C-RIP assays. Conversely, ALYREF overexpression significantly increased PD-L1 levels and enhanced m^5C binding to *PD-L1* mRNA. ALYREF is particularly critical in recognizing m^5C modifications and regulating mRNA stability [40, 41]. In our study, ALYREF-RIP analysis revealed enriched binding of *PD-L1* mRNA by ALYREF, an interaction that was diminished following NSUN2 knockdown and increased following ALYREF overexpression. These findings underscore the role of NSUN2 and ALYREF in stabilizing PD-L1 expression through m^5C modifications, thereby providing new insights into the

regulatory mechanisms linking m^5C RNA methylation with immune evasion in NSCLC.

We next investigated the effects of NSUN2 and ALYREF on the antitumor immune response in NSCLC cells. Upon coculturing NSCLC cells with activated $CD8^+$ T cells, we indicated that both NSUN2 and ALYREF provided protective effects for tumor cells against $CD8^+$ T-cell-mediated cytotoxicity. NSUN2 knockdown resulted in elevated levels of IFN-γ and TNF-α, while ALYREF overexpression suppressed these cytokines. A syngeneic mouse model corroborated these results, showing an inverse correlation between the NSUN2/ALYREF axis and $CD8^+$ T-cell infiltration in the tumor microenvironment. Our findings thus enriched the understanding of the function of m^5C writer and reader protein-mediated immunoregulation in NSCLC.

Our study also highlights the potential for combination therapies targeting NSUN2. Given its pivotal role in immune evasion, NSUN2 knockdown could sensitize tumors to immune checkpoint blockade, potentially overcoming resistance and enhancing therapeutic outcomes for NSCLC patients. Our findings on NSUN2-mediated m^5C methylation of *PD-L1* mRNA uncover novel insights into the role of RNA methylation in cancer immunotherapy. Therapeutic strategies targeting m^5C may modulate the immune response by regulating PD-L1 expression in cancer cells and influencing the function of immune cells, such as $CD8^+$ T cells. Specificity and toxicity assessment of NSUN2 inhibitors highlight the targeted inhibition of NSUN2 and suggest that the NSUN2 inhibitor has a selective cytotoxic effect on NSCLC cells. In vitro results from the combined use of the NSUN2 inhibitor and PD-1 inhibitor demonstrate that their co-administration enhances tumor cell cytotoxicity and improves T-cell-mediated killing. These findings provide preliminary validation of NSUN2 as a potential therapeutic target, laying the groundwork for its clinical application. However, while our in vitro and in vivo findings strongly support the role of NSUN2 and ALYREF in modulating PD-L1 expression and immune suppression, additional clinical studies are needed to evaluate the viability of targeting NSUN2 in NSCLC treatment. Future research should also investigate the broader implications of m^5C modification within the tumor microenvironment, including its potential as a predictive biomarker for patient response to immunotherapy.

In summary, our findings reveal a novel mechanism in which NSUN2 post-transcriptionally upregulates PD-L1 expression in an m^5C-ALYREF–dependent manner, enhancing *PD-L1* mRNA stability and promoting immune evasion in NSCLC. These insights deepen our understanding of the molecular basis of immune escape in NSCLC and suggest that NSUN2 and ALYREF may serve as promising therapeutic targets for improving the effectiveness of immune checkpoint inhibitors in NSCLC treatment.

Supplementary Information The online version contains supplementary material available at https://doi.org/10.1007/s00262-025-03986-5.

Acknowledgements Thanks go to all participants.

Author contributions YY and LC conceived and designed the research. YY, LC, XX, DL, YD, LL, JL, HJ, LS, YH, and YX carried out the experiments and analyzed the data. YY, XX, and LM wrote, reviewed, and edited the manuscript. YY, XX, YX, and LM supervised the research and provided funding support. All authors reviewed and approved the final manuscript.

Funding This study was supported by the National Natural Science Foundation of China (82472771, 82273139, 82303043, and 82373226), Shanghai Science and Technology Committee Rising-Star Program (22QA1408300), Talent Training Plan of Shanghai Chest Hospital in 2022 (RC-202301-130), and the High-level Local University Construction-Shanghai Jiao Tong University School of Medicine of Linghang pandeng Program (LHPD2304). Nurture projects for basic research of Shanghai Chest Hospital (2023YNJCQ2).

Data availability No datasets were generated or analyzed during the current study.

Declarations

Conflict of interest The authors declare that they have no potential conflict of interest.

Ethical approval The study had been approved by the ethics and research committees of the Shanghai Chest Hospital. All patients were duly informed before the samples collection, and written informed consent was received from each patient.

References

1. Bray F, Laversanne M, Sung H, Ferlay J, Siegel RL et al (2024) Global cancer statistics 2022: GLOBOCAN estimates of incidence and mortality worldwide for 36 cancers in 185 countries. CA Cancer J Clin 74:229–263. https://doi.org/10.3322/caac.21834
2. Sun Q, Hong Z, Zhang C, Wang L, Han Z et al (2023) Immune checkpoint therapy for solid tumours: clinical dilemmas and future trends. Signal Transduct Target Ther 8:320. https://doi.org/10.1038/s41392-023-01522-4

3. Pardoll DM (2012) The blockade of immune checkpoints in cancer immunotherapy. Nat Rev Cancer 12:252–264. https://doi.org/10.1038/nrc3239
4. Dong H, Strome SE, Salomao DR, Tamura H, Hirano F et al (2002) Tumor-associated B7–H1 promotes T-cell apoptosis: a potential mechanism of immune evasion. Nat Med 8:793–800. https://doi.org/10.1038/nm730
5. Adinew GM, Messeha SS, Taka E, Badisa RB, Soliman KFA (2022) Anticancer effects of thymoquinone through the antioxidant activity, upregulation of Nrf2, and downregulation of PD-L1 in triple-negative breast cancer cells. Nutrients 14(22):4787. https://doi.org/10.3390/nu14224787
6. Xiao D, Zeng T, Zhu W, Yu ZZ, Huang W et al (2023) ANXA1 promotes tumor immune evasion by binding PARP1 and upregulating Stat3-induced expression of PD-L1 in multiple cancers. Cancer Immunol Res 11:1367–1383. https://doi.org/10.1158/2326-6066.CIR-22-0896
7. Sun C, Mezzadra R, Schumacher TN (2018) Regulation and function of the PD-L1 checkpoint. Immunity 48:434–452. https://doi.org/10.1016/j.immuni.2018.03.014
8. Xue C, Chu Q, Zheng Q, Jiang S, Bao Z et al (2022) Role of main RNA modifications in cancer: N6-methyladenosine, 5-methylcytosine, and pseudouridine. Signal Transduct Target Ther 7:142. https://doi.org/10.1038/s41392-022-01003-0
9. Barbieri I, Kouzarides T (2020) Role of RNA modifications in cancer. Nat Rev Cancer 20:303–322. https://doi.org/10.1038/s41568-020-0253-2
10. Yang X, Yang Y, Sun B-F, Chen Y-S, Xu J-W et al (2017) 5-methylcytosine promotes mRNA export—NSUN2 as the methyltransferase and ALYREF as an m5C reader. Cell Res 27:606–625. https://doi.org/10.1038/cr.2017.55
11. Chen X, Li A, Sun B-F, Yang Y, Han Y-N et al (2019) 5-methylcytosine promotes pathogenesis of bladder cancer through stabilizing mRNAs. Nat Cell Biol 21:978–990. https://doi.org/10.1038/s41556-019-0361-y
12. Su J, Wu G, Ye Y, Zhang J, Zeng L et al (2021) NSUN2-mediated RNA 5-methylcytosine promotes esophageal squamous cell carcinoma progression via LIN28B-dependent GRB2 mRNA stabilization. Oncogene 40:5814–5828. https://doi.org/10.1038/s41388-021-01978-0
13. Hu Y, Chen C, Tong X, Chen S, Hu X et al (2021) NSUN2 modified by SUMO-2/3 promotes gastric cancer progression and regulates mRNA m5C methylation. Cell Death Dis 12:842. https://doi.org/10.1038/s41419-021-04127-3
14. Zhang X, An K, Ge X, Sun Y, Wei J et al (2024) NSUN2/YBX1 promotes the progression of breast cancer by enhancing HGH1 mRNA stability through m5C methylation. Breast Cancer Res 26:94. https://doi.org/10.1186/s13058-024-01847-0
15. Zou S, Huang Y, Yang Z, Zhang J, Meng M et al (2024) NSUN2 promotes colorectal cancer progression by enhancing SKIL mRNA stabilization. Clin Transl Med 14:e1621. https://doi.org/10.1002/ctm2.1621
16. Gao Y, Wang Z, Zhu Y, Zhu Q, Yang Y et al (2019) NOP2/Sun RNA methyltransferase 2 promotes tumor progression via its interacting partner RPL6 in gallbladder carcinoma. Cancer Sci 110:3510–3519. https://doi.org/10.1111/cas.14190
17. Lu L, Gaffney SG, Cannataro VL, Townsend J (2020) Transfer RNA methyltransferase gene NSUN2 mRNA expression modifies the effect of T cell activation score on patient survival in head and neck squamous carcinoma. Oral Oncol 101:104554. https://doi.org/10.1016/j.oraloncology.2019.104554
18. Xu X, Qiu S, Zeng B, Huang Y, Wang X et al (2024) N6-methyladenosine demethyltransferase FTO mediated m6A modification of estrogen receptor alpha in non-small cell lung cancer tumorigenesis. Oncogene 43:1288–1302. https://doi.org/10.1038/s41388-024-02992-8
19. Chen SY, Chen KL, Ding LY, Yu CH, Wu HY et al (2022) RNA bisulfite sequencing reveals NSUN2-mediated suppression of epithelial differentiation in pancreatic cancer. Oncogene 41:3162–3176. https://doi.org/10.1038/s41388-022-02325-7
20. Zhao Y, Xing C, Peng H (2024) ALYREF (Aly/REF export factor): a potential biomarker for predicting cancer occurrence and therapeutic efficacy. Life Sci 338:122372. https://doi.org/10.1016/j.lfs.2023.122372
21. Cho BC, Abreu DR, Hussein M, Cobo M, Patel AJ et al (2022) Tiragolumab plus atezolizumab versus placebo plus atezolizumab as a first-line treatment for PD-L1-selected non-small-cell lung cancer (CITYSCAPE): primary and follow-up analyses of a randomised, double-blind, phase 2 study. Lancet Oncol 23:781–792. https://doi.org/10.1016/S1470-2045(22)00226-1
22. Janjigian YY, Shitara K, Moehler M, Garrido M, Salman P et al (2021) First-line nivolumab plus chemotherapy versus chemotherapy alone for advanced gastric, gastro-oesophageal junction, and oesophageal adenocarcinoma (CheckMate 649): a randomised, open-label, phase 3 trial. Lancet 398:27–40. https://doi.org/10.1016/S0140-6736(21)00797-2
23. Li H, Li C-W, Li X, Ding Q, Guo L et al (2019) MET inhibitors promote liver tumor evasion of the immune response by stabilizing PDL1. Gastroenterology 156:1849-1861.e13. https://doi.org/10.1053/j.gastro.2019.01.252
24. Cui L, Ma R, Cai J, Guo C, Chen Z et al (2022) RNA modifications: importance in immune cell biology and related diseases. Signal Transduct Target Ther 7:334. https://doi.org/10.1038/s41392-022-01175-9
25. Tang Q, Li L, Wang Y, Wu P, Hou X et al (2023) RNA modifications in cancer. Br J Cancer 129:204–221. https://doi.org/10.1038/s41416-023-02275-1
26. Delaunay S, Helm M, Frye M (2024) RNA modifications in physiology and disease: towards clinical applications. Nat Rev Genet 25:104–122. https://doi.org/10.1038/s41576-023-00645-2
27. Shinoda S, Kitagawa S, Nakagawa S, Wei FY, Tomizawa K et al (2019) Mammalian NSUN2 introduces 5-methylcytidines into mitochondrial tRNAs. Nucleic Acids Res 47:8734–8745. https://doi.org/10.1093/nar/gkz575
28. Trixl L, Lusser A (2019) The dynamic RNA modification 5-methylcytosine and its emerging role as an epitranscriptomic mark. WIREs RNA 10:e1510. https://doi.org/10.1002/wrna.1510
29. Yang H, Wang Y, Xiang Y, Yadav T, Ouyang J et al (2022) FMRP promotes transcription-coupled homologous recombination via facilitating TET1-mediated m5C RNA modification demethylation. Proc Natl Acad Sci 119:e2116251119. https://doi.org/10.1073/pnas.2116251119
30. Zuo S, Li L, Wen X, Gu X, Zhuang A et al (2023) NSUN2-mediated m5C RNA methylation dictates retinoblastoma progression through promoting PFAS mRNA stability and expression. Clin Transl Med 13:e1273. https://doi.org/10.1002/ctm2.1273
31. Song D, An K, Zhai W, Feng L, Xu Y et al (2023) NSUN2-mediated mRNA m5C modification regulates the progression of hepatocellular carcinoma. Genom Proteomics Bioinform 21:823–833. https://doi.org/10.1016/j.gpb.2022.09.007
32. Wang Y, Wei J, Feng L, Li O, Huang L et al (2023) Aberrant m5C hypermethylation mediates intrinsic resistance to gefitinib through NSUN2/YBX1/QSOX1 axis in EGFR-mutant non-small-cell lung cancer. Mol Cancer 22:1–18. https://doi.org/10.1186/s12943-023-01780-4
33. Zhang X, Zhang Y, Li R, Li Y, Wang Q et al (2024) STUB1-mediated ubiquitination and degradation of NSUN2 promotes hepatocyte ferroptosis by decreasing m^5C methylation of Gpx4 mRNA. Cell Rep. https://doi.org/10.1016/j.celrep.2024.114885

34. Chen T, Xu ZG, Luo J, Manne RK, Wang Z et al (2023) NSUN2 is a glucose sensor suppressing cGAS/STING to maintain tumorigenesis and immunotherapy resistance. Cell Metab 35:1782-1798.e8. https://doi.org/10.1016/j.cmet.2023.07.009
35. Grivennikov SI, Greten FR, Karin M (2010) Immunity, inflammation, and cancer. Cell 140:883–899. https://doi.org/10.1016/j.cell.2010.01.025
36. Zhong Z, Sanchez-Lopez E, Karin M (2016) Autophagy, inflammation, and immunity: a troika governing cancer and its treatment. Cell 166:288–298. https://doi.org/10.1016/j.cell.2016.05.051
37. Yu G, Bao J, Zhan M, Wang J, Li X et al (2022) Comprehensive analysis of m5C methylation regulatory genes and tumor microenvironment in prostate cancer. Front Immunol. https://doi.org/10.3389/fimmu.2022.914577
38. Zhang J, Bu X, Wang H, Zhu Y, Geng Y et al (2018) Cyclin D-CDK4 kinase destabilizes PD-L1 via cullin 3–SPOP to control cancer immune surveillance. Nature 553:91–95. https://doi.org/10.1038/nature25015
39. Koh J, Lee D, Kim S, Song SG, Han B et al (2024) Spatially resolved whole-transcriptomic and proteomic profiling of lung cancer and its immune-microenvironment according to PD-L1 expression. Cancer Immunol Res. https://doi.org/10.1158/2326-6066.cir-24-0071
40. Jin Y, Yao J, Fu J, Huang Q, Luo Y et al (2024) ALYREF promotes the metastasis of nasopharyngeal carcinoma by increasing the stability of NOTCH1 mRNA. Cell Death Dis 15:578. https://doi.org/10.1038/s41419-024-06959-1
41. Wang J-Z, Zhu W, Han J, Yang X, Zhou R et al (2021) The role of the HIF-1α/ALYREF/PKM2 axis in glycolysis and tumorigenesis of bladder cancer. Cancer Commun 41:560–575. https://doi.org/10.1002/cac2.12158